Int. J. Electrochem. Sci., 14 **(2019)** 10920 – 10930, doi: 10.20964/2019.12.27

International Journal of
ELECTROCHEMICAL
SCIENCE
www.electrochemsci.org

Short Communication

Preparation of lithium $Li_4Ti_5O_{12}$-graphene composite as cathode for improving lithium battery performance

Zhonghao Gu and Donglin Tang[*]

School of Mechatronic Engineering, Southwest Petroleum University, Chengdu, Sichuan 610500 P.R. China
[*]E-mail: qinmenransj@163.com

Received: 12 July 2019 / *Accepted:* 19 September 2019 / *Published:* 29 October 2019

Nanocrystallization and morphological control of $Li_4Ti_5O_{12}$ have always been the focus of many researchers. The conductivity of $Li_4Ti_5O_{12}$ can be greatly improved by the nano-effect and the reduction of the transmission distance of Li^+ ions. Spherical $Li_4Ti_5O_{12}$ was prepared by a sol-gel method and a hydrothermal method. First, SiO_2 nanoparticles were used as templates to prepare SiO_2-TiO_2 composites by the sol-gel method. Then, $Li_4Ti_5O_{12}$ was synthesized by the hydrothermal method using LiOH as the lithium source. The internal SiO_2 was removed by the corrosive effect of LiOH. Carbon doping and coating modification of $Li_4Ti_5O_{12}$ have always been an important direction for the modification of $Li_4Ti_5O_{12}$. The high conductivity of carbon materials can further improve the rate performance of $Li_4Ti_5O_{12}$. Therefore, graphene oxide was wrapped around the prepared spherical $Li_4Ti_5O_{12}$ surface at room temperature. Then, hollow $Li_4Ti_5O_{12}$-graphene composites were synthesized by high-temperature calcination. The effects of different graphene contents on the D/G band ratio and cycling properties of the composites were studied.

Keywords: $Li_4Ti_5O_{12}$; Graphene; Cathode; Lithium battery; Nanocomposite

1. INTRODUCTION

In recent years, environmental pollution and energy crises have gradually become two major challenges facing sustainable human development. With the rapid development of population and industrialization, the existing non-renewable resources cannot meet the needs of long-term economic development [1–7]. In addition, the traditional sources of fossil energy pose serious environmental problems. Therefore, the development of renewable clean new energy has become the main aim of current scientific researchers. A chemical power supply is a device that can convert and store chemical energy and electric energy and plays an important role as a bridge in the rational use of various new green energy sources. The development of a chemical power supply has important practical significance

in solving the energy crisis and environmental pollution problems [8–12]. Traditional chemical power sources include lead-acid batteries, nickel-chromium batteries and nickel-hydrogen batteries [13–18]. However, due to their low energy density, serious environmental pollution and high self-discharge defects, the traditional batteries cannot meet the needs for the sustainable development of society [19–25]. As a new type of green power supply, lithium-ion batteries have been the focus of attention from many fields of study since their advent [26–30]. Compared with traditional batteries, lithium batteries have the advantages of being lightweight along with having a small volume, high energy density, long service life, no memory effect and environmental friendliness. In recent years, Li-ion batteries have occupied a large share of the small secondary battery market and are widely used in mobile phones, laptops, digital cameras and other electronic products [31–35].

At present, commercial cathode materials for lithium ion batteries are mainly carbon materials, but there are many problems in the application of carbon materials, such as short cycle performance, safety and low rate performance. In recent years, researchers have developed new cathode materials, including silicon-based materials, alloy materials, transition metal oxides and metal nitrides. The development of cathode materials determines the development of lithium-ion batteries [36–41]. The successful commercialization of lithium-ion batteries is attributed to the successful application of carbon materials as cathode materials for lithium-ion batteries. A large number of studies have successfully explored the lithium intercalation mechanism of carbon materials. This mechanism is the precondition for the study of carbon materials as cathode materials. The microstructures of carbon materials determine their good lithium intercalation and subsequent lithium removal properties [42–44].

Carbon-negative electrode materials have low electrode potential, good safety and cycle life and can meet the current lithium charging and discharging requirements. The theoretical specific capacity of general carbon materials is between 200 and 400 mAh/g. The theoretical specific capacity of graphitized carbon can reach 372 mAh/g. Therefore, the current lithium-ion battery cathode materials are basically carbon materials. Because graphite has a high theoretical specific capacity, commercial carbon cathode materials are mainly graphite. In recent years, new carbon materials (graphene, carbon nanotubes) have become the hotspot of people's ingenuity. It was found that graphene and carbon nanotubes have high theoretical specific capacity, and the first discharge capacity of carbon nanotubes can reach 1229 mAh/g. However, carbon materials have many shortcomings, such as an electrode potential close to that of metal, and the voltage lag phenomenon is obvious, which will cause safety problems when the battery is overcharged. In addition, the volume effect of carbon materials is limited. In the process of charging and discharging, with lithium ions repeatedly intercalated in carbon materials, the microstructure of carbon materials changes, resulting in poor cycle stability and a decline in energy density [45–49].

$Li_4Ti_5O_{12}$ is a new negative electrode material for lithium-ion batteries. Because of its small volume effect, the volume change before and after charging and discharging is only 0.3%. Therefore, $Li_4Ti_5O_{12}$ is called a "zero strain" material and has excellent cycling performance. In addition, the charging and discharging voltage platform of $Li_4Ti_5O_{12}$ is long and stable, and the material can discharge fully when the discharge voltage is satisfied [50–53]. In addition, the industrial production process of $Li_4Ti_5O_{12}$ is simple, and the production cost is low. Compared with other carbon cathode material, $Li_4Ti_5O_{12}$ has better safety and cycle performance. Compared with silicon-based materials, it has better recycling performance, a simpler preparation process and a cheaper price.

$Li_4Ti_5O_{12}$ has obvious shortcomings as a cathode material for lithium-ion batteries, such as a low voltage of single batteries due to its high potential. $Li_4Ti_5O_{12}$ has poor conductivity and low ionic conductivity, which further limits its commercial application. The modification methods of $Li_4Ti_5O_{12}$ mainly include the following: (1) synthesis of nano-sized $Li_4Ti_5O_{12}$ materials; (2) synthesis of $Li_4Ti_5O_{12}$ materials with a special morphology and porous structure; (3) doping modification of metal ions; (4) carbon coating modification; and (5) composite modification of transition metal oxides. In recent years, research on $Li_4Ti_5O_{12}$ has mainly focused on the nanocrystallization of $Li_4Ti_5O_{12}$ materials and the preparation of different morphologies and doping modifications. These studies have improved the rate performance and charge-discharge capacity of $Li_4Ti_5O_{12}$. Therefore, this paper further studies $Li_4Ti_5O_{12}$ to improve the D/G band ratio performance and energy density of pure phase $Li_4Ti_5O_{12}$ and its composites.

2. EXPERIMENTAL

Tetra-n-butyl titanate, hydroxypropyl cellulose, ferric chloride hexahydrate, tetraethoxysilane and lithium hydroxide monohydrate were purchased from Sinopharm Co. Ltd. All other chemicals were of analytical grade.

Preparation of SiO_2 nanomaterials: Monodispersed SiO_2 nanoparticles were synthesized by an improved Stober method. First, three solutions of A, B and C were prepared. For solution A, 1.6 mL TEOS was added to 44 mL absolute ethanol, while solution B used 10 mL ammonia water added to 44 mL absolute ethanol, and solution C used 2 mL TEOS added to 88 mL absolute ethanol. Next, solution A and solution B were mixed for 0.5 h and then 8 mL ammonia water was added and stirred for 10 min. The monodispersed SiO_2 was obtained by adding solution C to the mixture with centrifugal washing after reacting for 2 h.

Preparation of SiO_2-TiO_2 nanoparticles: An amount of 0.2 g SiO_2 was ultrasonically dispersed in the mixed solution (0.1 g hydroxypropyl cellulose, 60 mL anhydrous ethanol, and 0.6 g of deionized water). The above mixture was stirred at room temperature for 2 h, and then a vacuum injection pump was used to drop 6 mL of a tetrabutyl orthotitanate mixed solution with ethanol (TBOT: ethanol = volume ratio 1/5) at a speed of 0.5 mL/min and stirred at room temperature for 40 min. Then the mixture was heated up to 80℃ and refluxed for 100 min. Centrifuge separation was used to obtain the product, and then it was finally dispersed in 15 mL anhydrous ethanol.

Preparation of spherical $Li_4Ti_5O_{12}$: The synthesized SiO_2-TiO_2 ethanol solution was further mixed with 30 mL LiOH (0.5 M) and placed in a 50 mL polytetrafluoroethylene reactor. The reaction was carried out in a drying oven with air blowing and at 160℃ for 6 h. After the reaction was reduced to room temperature, the product was deionized and washed to neutral. The product was dried at 60℃ for 6 h to obtain a white powder. The product was then placed in a crucible and calcined in a muff furnace for 4 h at 300℃ or 600℃.

Preparation of $Li_4Ti_5O_{12}$-graphene composite: $Li_4Ti_5O_{12}$ was first dispersed into water to form a concentration of 1 mg/mL. Then, a certain amount of graphene oxide was added into the dispersion and

stirred for 3 h. The mixture was filtered, and the solid was calcined at 500℃ under N_2 conditions for 2 h.

The electrochemical performance characterization was carried out using a conventional lithium button battery system.

3. RESULTS AND DISCUSSION

Figure 1A shows the SEM image of the prepared $Li_4Ti_5O_{12}$. As shown in the figure, the prepared $Li_4Ti_5O_{12}$ exhibits a spherical shape with a similar size. Figure 1B shows the XRD characterization of the spherical hollow $Li_4Ti_5O_{12}$ obtained by calcining. It can be seen from the figure that there are obvious diffraction peaks at 18.31, 35.61, 43.14, 57.27 and 62.81 for the two curves and these belong to the crystal planes (111), (311), (400), (333) and (440) of $Li_4Ti_5O_{12}$, respectively. The half-peak width of the diffraction peak of $Li_4Ti_5O_{12}$ calcined at 600℃ is obviously smaller than that of $Li_4Ti_5O_{12}$ calcined at 300℃, indicating that the agglomeration of $Li_4Ti_5O_{12}$ nanoparticles calcined at 600℃ is larger. In addition, the $Li_4Ti_5O_{12}$ calcined at 600℃ also shows obvious diffraction peaks at 47.32, 66.27, 74.14 and 79.21, while the $Li_4Ti_5O_{12}$ calcined at 300℃ has no obvious diffraction peaks, indicating that the crystal shape of $Li_4Ti_5O_{12}$ calcined at 600℃ is significantly better than that of the $Li_4Ti_5O_{12}$ calcined at 300℃. Figure 1C shows the XRD pattern of $Li_4Ti_5O_{12}$-graphene. It can be seen from the pattern that there is still a $Li_4Ti_5O_{12}$ phase in the diffraction peak. However, the addition of graphene reduced the intensity for each diffraction peak of $Li_4Ti_5O_{12}$. However, in the spectra of $Li_4Ti_5O_{12}$-graphene, the G band broadens while the D band expands, corresponding to the enlarging of sp^3 domains. The increased D/G band ratio can be attributed to the formation of new graphitic domains and the average size contraction of sp^2 domains [54]. When large amounts of graphene are present, the diffraction peaks at 57.21 and 66.27 no longer exist. With the increase in the content of coated graphene, the strength of each diffraction peak of $Li_4Ti_5O_{12}$ significantly decreases, and the crystal shape becomes worse.

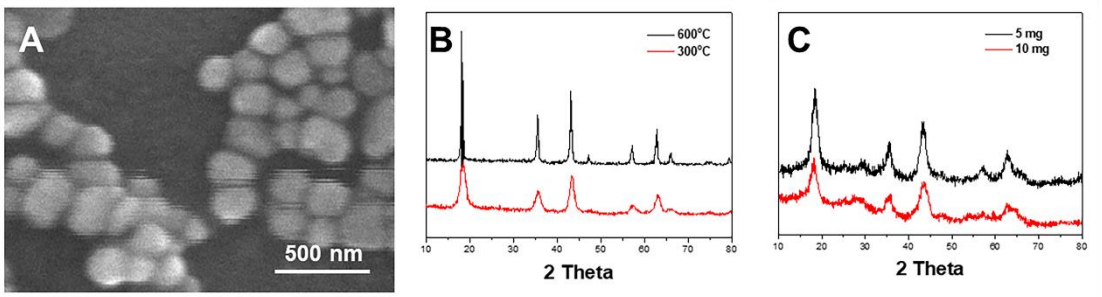

Figure 1. (A) SEM image of $Li_4Ti_5O_{12}$. (B) XRD patterns of $Li_4Ti_5O_{12}$ prepared at 300℃ and 600℃. (C) XRD patterns of $Li_4Ti_5O_{12}$-graphene with different graphene content.

Figure 2A is the CV diagram of the two-electrode system after $Li_4Ti_5O_{12}$ is assembled into button cells prepared at 600℃. The potential range of the test is 0 ~ 3 V, and the sweep speed is 0.2 mV/s. It can be seen from the figure that the redox peak is relatively symmetrical, which indicates that lithium ions have a relatively good transfer rate in spherical hollow $Li_4Ti_5O_{12}$. It is obvious from the figure that

the charging potential platform of $Li_4Ti_5O_{12}$ is approximately 1.6 V, while the discharging potential platform is approximately 1.5 V. Hence, the diffusion path is significantly shortened for both lithium ions and electrons when such composites are used as the cathode material for lithium-ion batteries [55]. Figure 2B shows the CV diagram of the two-electrode system tested after the $Li_4Ti_5O_{12}$-graphene composite material was assembled into the button battery. From the figure, it can be seen that the redox peak is relatively symmetrical, which indicates that $Li_4Ti_5O_{12}$-graphene has a better transfer rate for lithium ions. After the first curve, the peak strength and peak level changed slightly, which may be because the battery was activated after a round of charging and discharging, and the whole battery system changed. The $Li_4Ti_5O_{12}$-graphene additive can significantly increase the content of active lithium during the initial delithiation process, which is conducive to the formation of a stable passivation film on the anode surface and the achievement of a stable discharge capacity in these cycles [56–60]. The peak patterns of the two cycles coincide, and the redox peaks are relatively symmetrical, which indicates that the cycling performance of the battery is relatively stable after one cycle.

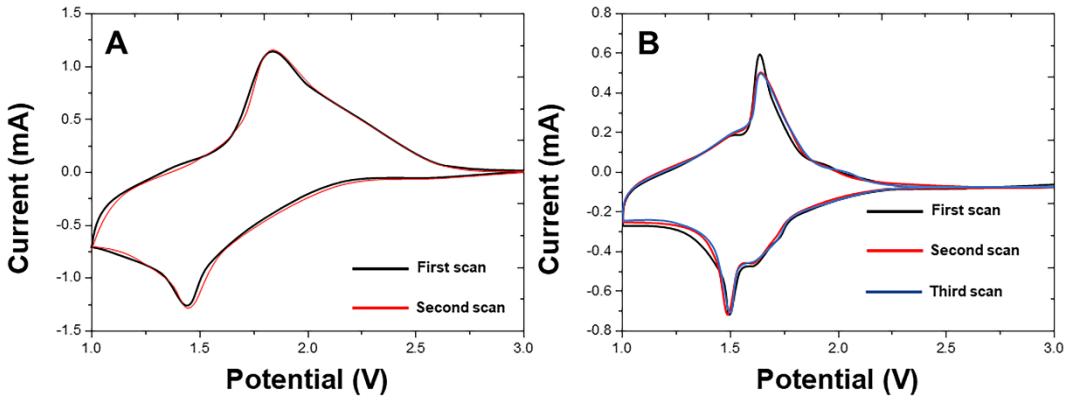

Figure 2. (A) First and second CV curves of the prepared $Li_4Ti_5O_{12}$. (B) First three CV curves of the prepared $Li_4Ti_5O_{12}$-graphene.

The electrochemical properties of the two samples were investigated by galvanostatic charge/discharge testing. Figure 3 shows the galvanostatic charge/discharge curves of the $Li_4Ti_5O_{12}$-graphene samples at a current density of 0.2 C within a voltage range of 3.5–4.95 V. Two pairs of charge/discharge plateaus can be observed at approximately 4.3–4.9 V, associated with the Ti^{2+}/Ti^{6+} redox processes in $Li_4Ti_5O_{12}$-graphene. The charge/discharge plateaus in the charge–discharge curves are in agreement with the redox peaks observed in CV curves.

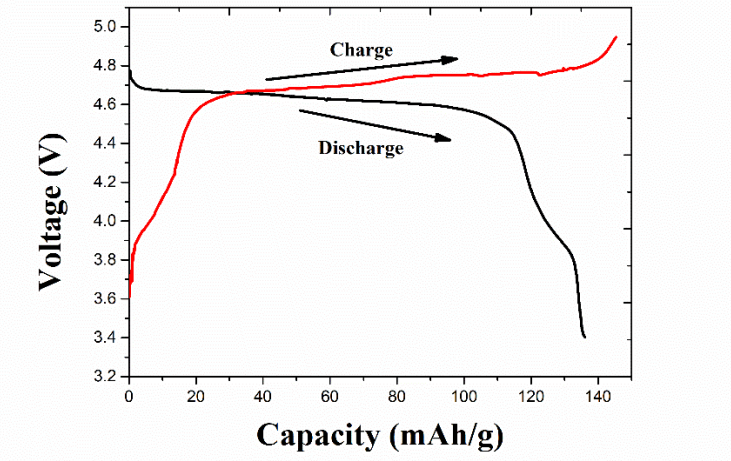

Figure 3. Galvanostatic charge/discharge curves of the prepared $Li_4Ti_5O_{12}$-graphene at 0.2 C.

The cycling performance of $Li_4Ti_5O_{12}$ after calcining at 300℃ and 600℃ is shown in Figure 4A. As seen from the figure, the specific discharge capacity of $Li_4Ti_5O_{12}$ after calcining at 300℃ and 600℃ is 175 mAh/g and 174 mAh/g, respectively; after 250 cycles, the capacity is 160 mAh/g and 155 mAh/g, respectively, and the capacity retention rates are 91% and 89%, respectively. It can be seen that the cycling performance of $Li_4Ti_5O_{12}$ calcined at 600℃ is better than that of $Li_4Ti_5O_{12}$ calcined at 300℃. Because the $Li_4Ti_5O_{12}$-graphene additive releases almost all active lithium ions to compensate for the lithium loss due to the formation of solid electrolyte interphase on the anode surface during the first charge, $Li_4Ti_5O_{12}$-graphene achieves improved cycling stability [25,61–63]. We then assembled the $Li_4Ti_5O_{12}$-graphene composite material into the battery and tested its cycling performance at 5 C. As shown in the cycling performance curve in Figure 4B, the specific discharge capacity of the 5 mg graphene composite material was 150 mAh/g at 5 C and 146 mAh/g after 350 cycles. The 10 mg graphene composite had a specific discharge capacity of 157 mAh/g at 5 C, and the discharge capacity was still 122 mAh/g after 350 cycles.

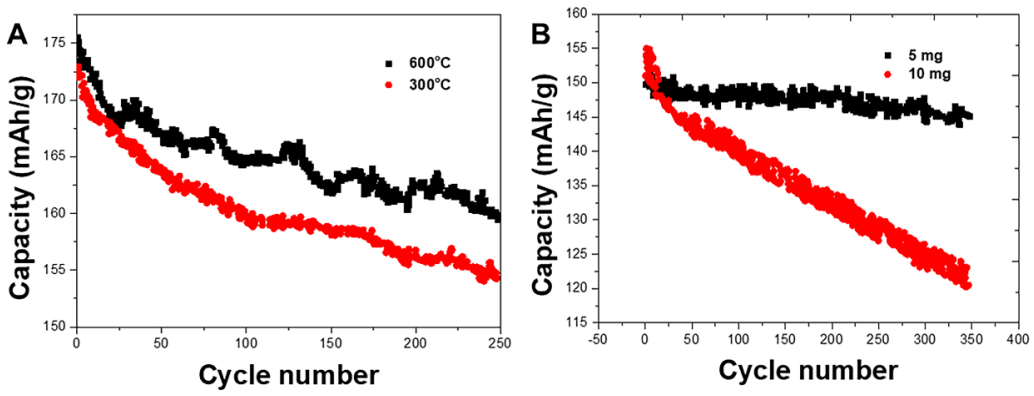

Figure 4. (A) The cycling performance of $Li_4Ti_5O_{12}$ with different calcination temperature under the charge and discharge rate of 1 C. (B) The cycling performance of the $Li_4Ti_5O_{12}$-graphene composite with different graphene contents after calcination under the charge and discharge rate of 5 C.

Figure 5A shows the charging and discharging tests of $Li_4Ti_5O_{12}$ calcined at different temperatures and assembled into button batteries with 0.2 C, 1 C, 2 C, 5 C and 10 C. The specific capacity of the material at 600℃ is 168 mAh/g at 0.2 C, which is close to the theoretical specific capacity of $Li_4Ti_5O_{12}$ and is higher than 161 mAh/g at 300℃. It can be seen from the figure that the specific capacity of the material decreases rapidly when the multiplying power increases. When the multiplying power is increased to 10 C, the specific discharge capacity is only 46 mAh/g. The specific capacity decreasing with increasing multiplying power phenomenon may be due to the polarization of the electrodes. With the increase of multiplying power, the current increases, and the mobility of Li^+ increases as well. However, Li^+ has a certain diffusion coefficient in $Li_4Ti_5O_{12}$. When the diffusion rate is too low, the polarization of the electrode results in the battery reaching the cut-off voltage faster when discharging, so the specific capacity is lower. Li^+ requires rapid diffusion when charging or discharging at high current. However, the transmission channels decrease and diffuse. Therefore, Li^+ has difficulty entering the core reaction or enters the core with high energy loss, resulting in more specific capacity reduction.

Figure 5B shows the charging and discharging tests of $Li_4Ti_5O_{12}$-graphene with different graphene contents and assembled into button batteries with 0.2 C, 1 C, 2 C, 5 C and 10 C. The addition of graphene significantly improves the cycling performance of the cathode. In addition, 5 mg graphene showed a superior performance compared with that of the 10 mg graphene.

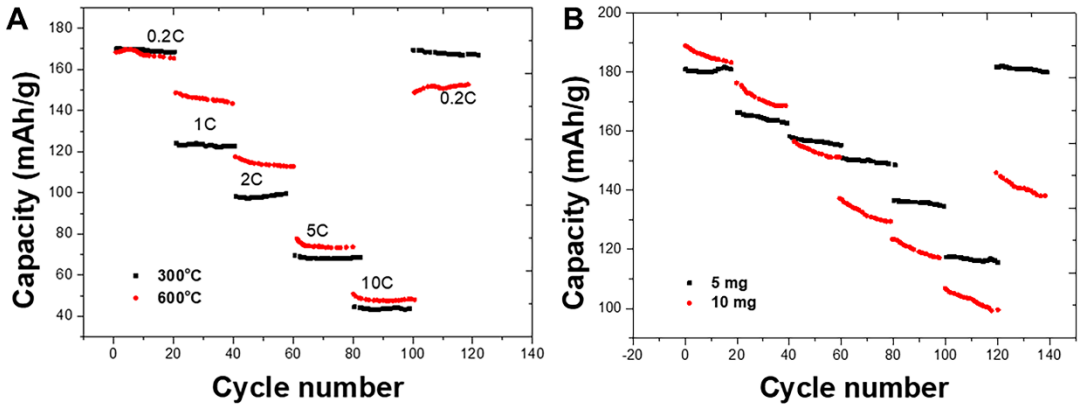

Figure 5. (A) Cycling performance of $Li_4Ti_5O_{12}$ with different calcination temperature under different charge-discharge multiplying powers. (B) Cycling performance of the $Li_4Ti_5O_{12}$-graphene composite with different graphene contents after calcination under different charge-discharge multiplying powers.

The electrochemical impedance was used to measure $Li_4Ti_5O_{12}$ and $Li_4Ti_5O_{12}$-graphene. As shown in Figure 6, the high frequency semicircle diameter of the prepared $Li_4Ti_5O_{12}$-graphene composite is smaller, and the interfacial resistance is much lower than that of $Li_4Ti_5O_{12}$. This result further confirms that the $Li_4Ti_5O_{12}$-graphene composite has better conductivity than $Li_4Ti_5O_{12}$. Therefore, electrons can be easily transmitted in the channel of the cathode material. In addition, it is conducive to the transfer of lithium ions between the electrode surface and the electrolyte.

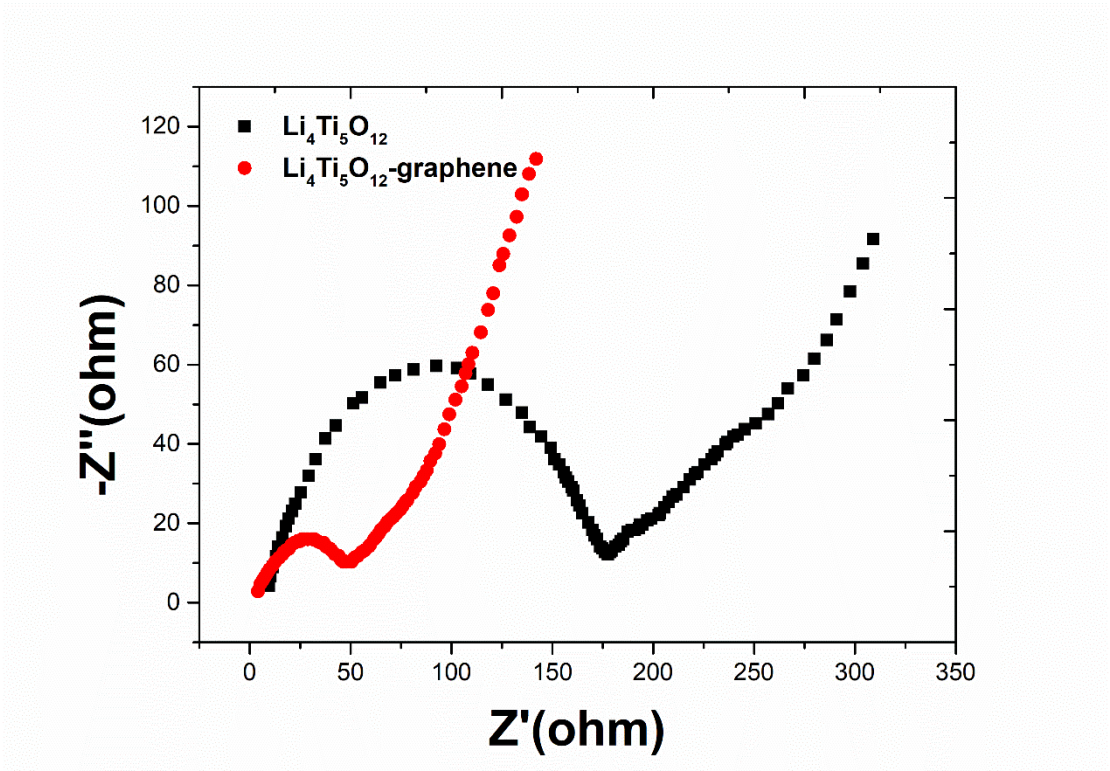

Figure 6. The electrochemical impedance spectra of $Li_4Ti_5O_{12}$ and $Li_4Ti_5O_{12}$-graphene.

Table 1 shows the electrochemical properties of similar cathode materials used in lithium-ion batteries. As shown in Table 1, it is clear that among these similar cathode materials, $Li_4Ti_5O_{12}$-graphene composites have excellent cycling stability. This indicates that the $Li_4Ti_5O_{12}$-graphene composite material will be a promising cathode material for lithium-ion batteries.

Table 1. Comparison between the $Li_4Ti_5O_{12}$-graphene composite and other similar cathode materials.

Material	Current Density	Capacity	Reference
Zn-doped $Li_4Ti_5O_{12}$	0.2 C	179 mAh/g	[64]
$LiCoMnO_4/Li_4Ti_5O_{12}$	0.2 C	202 mAh/g	[65]
Carbon-coated $Li_4Ti_5O_{12}$	0.2 C	187 mAh/g	[66]
$LiMn_2O_4/Li_4Ti_5O_{12}$	0.2 C	178 mAh/g	[67]
$Li_4Ti_5O_{12}$-graphene composite	0.2 C	189 mAh/g	This work

4. CONCLUSION

$SiO_2@TiO_2$ with good dispersibility was successfully synthesized by high-temperature reflux using the sol-gel method. SiO_2 was used as a template after modifying with hydroxypropyl cellulose on its surface. Then, the $Li_4Ti_5O_{12}$ precursor was synthesized by a hydrothermal method using LiOH as the

lithium source. The corrosive effect of LiOH was used to remove the internal SiO_2. Then, a calcination process with different temperatures was used for $Li_4Ti_5O_{12}$ preparation. The electrochemical properties of $Li_4Ti_5O_{12}$ at different calcination temperatures were studied. As the temperature increased from 300℃ to 600℃, the crystal shape of $Li_4Ti_5O_{12}$ improved. The voltage platform of calcined lithium titanate at 600℃ was obviously superior to that of calcined $Li_4Ti_5O_{12}$ at 300℃. Graphene was then added to $Li_4Ti_5O_{12}$ to improve the performance. Graphene oxide was coated on the prepared $Li_4Ti_5O_{12}$ by using electrostatic forces and stirring at room temperature. $Li_4Ti_5O_{12}$-graphene composite materials with different reduced graphene contents were synthesized by high-temperature calcination.

References

1. Z. Al-Hamamre, M. Saidan, M. Hararah, K. Rawajfeh, H.E. Alkhasawneh, M. Al-Shannag, *Renew. Sustain. Energy Rev.*, 67 (2017) 295–314.
2. A. Adharis, D. Vesper, N. Koning, K. Loos, *Green Chem.* (2018) 10.1039.C7GC03023A.
3. A. Hamidi, D. Nazarpour, S. Golshannavaz, *Int. J. Energy Res.*, 42 (2017).
4. S.Y. Abujarad, M.W. Mustafa, J.J. Jamian, *Renew. Sustain. Energy Rev.*, 70 (2017) 215–223.
5. M. Jiang, J. Ma, M. Wu, R. Liu, L. Liang, F. Xin, W. Zhang, H. Jia, W. Dong, *Bioresour. Technol.*, 245 (2017) 1710.
6. H. Hassanzadehfard, A. Jalilian, *Int. J. Green Energy*, 15 (2018) 1–16.
7. Y.S. Prasad, S. Miryala, K. Lalitha, K. Ranjitha, S. Barbhaiwala, V. Sridharan, C.U. Maheswari, C.S. Srinandan, S. Nagarajan, *Acs Appl. Mater. Interfaces*, 9 (2017) 40047.
8. N. Violante, O. Senofonte, G. Marsili, P. Meli, M.E. Soggiu, S. Caroli, *Microchem. J.*, 67 (2000) 397–405.
9. Nighat, Farah, Mahmooduzzafar, Iqbal, Muhammad, *Biologia (Bratisl.)*, 63 (2008) 1128–1134.
10. D. Sheehan, J. Mcintosh, A. Power, P.J. Fitzpatrick, *Biochem. Soc. Trans.*, 23 (1995) 419.
11. M. Ahlberg, L. Berghem, G. Nordberg, S.A. Persson, L. Rudling, B. Steen, *Environ. Health Perspect.*, 47 (1983) 85–102.
12. C.M. González, M.L. Pignata, L. Orellana, *Sci. Total Environ.*, 312 (2003) 245–253.
13. J. Yang, H. Chen, W. Hao, Y. Kai, B.L. Jing, Y. Hui, *Int. J. Energy Res.*, 41 (2017).
14. M.A. Deyab, *J. Power Sources*, 390 (2018) 176–180.
15. R.J. Noll, J.M. Hughes, *J. Chem. Educ.*, 95 (2018) 852–857.
16. S.P. Ayeng'O, T. Schirmer, K.P. Kairies, H. Axelsen, D.U. Sauer, *Sol. Energy*, 162 (2018) 140–152.
17. J. Lach, K. Wróbel, J. Wróbel, P. Podsadni, A. Czerwiński, *J. Solid State Electrochem.*, 23 (2019) 693–705.
18. J. Büngeler, E. Cattaneo, B. Riegel, D.U. Sauer, *J. Power Sources*, 375 (2018) 53–58.
19. L. Fu, G. Chen, N. Jiang, J. Yu, C.-T. Lin, A. Yu, *J. Mater. Chem. A*, 4 (2016) 19107–19115.
20. L. Fu, Z. Fu, *Ceram. Int.*, 41 (2015) 2492–2496.
21. F. Han, H. Li, J. Yang, X. Cai, L. Fu, *Phys. E Low-Dimens. Syst. Nanostructures*, 77 (2016) 122–126.
22. F. Han, H. Li, L. Fu, J. Yang, Z. Liu, *Chem. Phys. Lett.*, 651 (2016) 183–187.
23. Y. Zheng, L. Fu, F. Han, A. Wang, W. Cai, J. Yu, J. Yang, F. Peng, *Green Chem. Lett. Rev.*, 8 (2015) 59–63.
24. L. Fu, Y. Zheng, P. Zhang, H. Zhang, M. Wu, H. Zhang, A. Wang, W. Su, F. Chen, J. Yu, *Bioelectrochemistry* (2019).
25. L. Fu, Y. Zheng, P. Zhang, H. Zhang, W. Zhuang, H. Zhang, A. Wang, W. Su, J. Yu, C.-T. Lin, *Biosens. Bioelectron.*, 120 (2018) 102–107.
26. F. Yang, W. Dong, Y. Xing, K.L. Tsui, *Microelectron. Reliab.*, 70 (2017) 70–78.
27. S. Deng, Z. Li, *Integr. Ferroelectr.*, 182 (2017) 10–20.

28. T. Zahid, K. Xu, W. Li, *Electron. Lett.*, 53 (2018) 1665–1666.
29. X. Su, W. Shuai, M. Pecht, L. Zhao, Y. Zhe, *Microelectron. Reliab.*, 70 (2017) 59–69.
30. L. Song, F. Tang, Z. Xiao, C. Zhong, H. Zhu, A. Li, *J. Electron. Mater.*, 47 (2018) 5896–5904.
31. A. GhavamiNejad, C.H. Park, C.S. Kim, *Biomacromolecules*, 17 (2016) 1213–1223.
32. B. Bari, J. Lee, T. Jang, P. Won, S.H. Ko, K. Alamgir, M. Arshad, L.J. Guo, *J. Mater. Chem. A*, 4 (2016) 11365–11371.
33. M. Javanbakht, M.R. Ganjali, P. Norouzi, A. Badiei, A. Hasheminasab, M. Abdouss, *Electroanal. Int. J. Devoted Fundam. Pract. Asp. Electroanal.*, 19 (2007) 1307–1314.
34. L. Fu, G. Lai, G. Chen, C.-T. Lin, A. Yu, *ChemistrySelect*, 1 (2016) 1799–1803.
35. L. He, L. Fu, Y. Tang, *Catal. Sci. Technol.*, 5 (2015) 1115–1125.
36. H. Zhang, Chenmzcioc.Ac. Cn, *J. Energy Chem.*, v.27 (2018) 223–230.
37. W. Feng, Q. Xue, L. Li, X. Zhang, Y. Huang, E. Fan, R. Chen, *Rsc Adv.*, 7 (2017) 1191–1199.
38. Y. Ma, A. Huang, H. Zhou, S. Ji, S. Zhang, R. Li, H. Yao, X. Cao, P. Jin, *J. Mater. Chem. A*, 5 (2017).
39. C. Zhu, Z. Wu, X. Jian, C. Zhen, T. Jian, G. Cao, X. Zhao, *J. Mater. Sci. Technol.*, 34 (2018) 92–97.
40. Y.T. Chen, H.Y. Zhang, Y.M. Chen, G. Qin, X.L. Lei, L.Y. Liu, *Mater. Sci. Forum*, 913 (2018) 818–830.
41. L. Xing, G. Gao, Y. Liu, Z. Ge, P. Leng, G. Wu, *J. Sol-Gel Sci. Technol.*, 82 (2017) 1–9.
42. H. Yin, X.X. Yu, H. Zhao, C. Li, M.Q. Zhu, *J. Solid State Electrochem.*, 22 (2018) 2395–2403.
43. P. Hao, T. Zhu, Q. Su, J. Lin, R. Cui, X. Cao, Y. Wang, A. Pan, *Front. Chem.*, 6 (2018) 195-.
44. T. Zhao, R. Ji, Y. Meng, G. Zhang, H. Si, Y. Wang, M. Yang, F. Wu, L. Li, R. Chen, *J. Mater. Sci.*, 54 (2019) 9098–9110.
45. P. Hui, Z. Cheng, Z. Xiao, X. Li, R. Wang, *Adv. Funct. Mater.*, 27 (2017) 1703936.
46. B. Ali, A. Ur-Rehman, F. Ghafoor, M.I. Shahzad, S.K. Shah, S.M. Abbas, *J. Power Sources*, 396 (2018) 467–475.
47. A.N. Krasnovskii, P.S. Kishchuk, *Russ. J. Appl. Chem.*, 90 (2017) 721–725.
48. X. Sun, W. Jie, L. Xu, C. Wei, *J. Nanoparticle Res.*, 20 (2018) 13.
49. M.I. Ionescu, *Rsc Adv.*, 7 (2017) 30365–30369.
50. S. Repp, E. Harputlu, S. Gurgen, M. Castellano, N. Kremer, N. Pompe, J. Wörner, A. Hoffmann, R. Thomann, F.M. Emen, *Nanoscale*, 7 (2018) 11222.
51. R. Dedryvère, D. Foix, S. Franger, S. Patoux, L. Daniel, D. Gonbeau, *J. Phys. Chem. C*, 114 (2017) 10999–11008.
52. M. Gockeln, S. Pokhrel, F. Meierhofer, J. Glenneberg, M. Schowalter, A. Rosenauer, U. Fritsching, M. Busse, L. Mädler, R. Kun, *J. Power Sources*, 374 (2018) 97–106.
53. D. Farhat, F. Ghamouss, J. Maibach, K. Edström, D. Lemordant, *Chemphyschem*, 18 (2017) 1333.
54. R. Arsat, M. Breedon, M. Shafiei, P. Spizziri, S. Gilje, R. Kaner, K. Kalantar-zadeh, W. Wlodarski, *Chem. Phys. Lett.*, 467 (2009) 344–347.
55. X. Fan, Y. Zhu, C. Luo, T. Gao, L. Suo, S.-C. Liou, K. Xu, C. Wang, *J. Power Sources*, 307 (2016) 435–442.
56. Y. Sun, H.-W. Lee, Z.W. Seh, N. Liu, J. Sun, Y. Li, Y. Cui, *Nat. Energy*, 1 (2016) 15008.
57. L. Fu, Z. Liu, J. Ge, M. Guo, H. Zhang, F. Chen, W. Su, A. Yu, *J. Electroanal. Chem.*, 841 (2019) 142–147.
58. Y. Zheng, Z. Wang, F. Peng, L. Fu, *Rev. Mex. Ing. Quím.*, 16 (2017).
59. Y. Zheng, Z. Wang, F. Peng, A. Wang, X. Cai, L. Fu, *Fuller. Nanotub. Carbon Nanostructures*, 24 (2016) 149–153.
60. Y. Zheng, H. Zhang, L. Fu, *Inorg. Nano-Met. Chem.*, 48 (2018) 449–453.
61. Y. Zheng, Z. Wang, F. Peng, L. Fu, *Inorg. Nano-Met. Chem.*, 47 (2017) 934–937.
62. Y. Zheng, A. Wang, W. Cai, Z. Wang, F. Peng, Z. Liu, L. Fu, *Enzyme Microb. Technol.*, 95 (2016) 112–117.

63. Y. Zheng, L. Fu, A. Wang, W. Cai, *Int J Electrochem Sci*, 10 (2015) 3530–3538.
64. B. Zhang, H. Du, B. Li, F. Kang, *Electrochem. Solid-State Lett.*, 13 (2010) A36–A38.
65. X. Huang, M. Lin, Q. Tong, X. Li, Y. Ruan, Y. Yang, *J. Power Sources*, 202 (2012) 352–356.
66. G. Wang, J. Gao, L. Fu, N. Zhao, Y. Wu, T. Takamura, *J. Power Sources*, 174 (2007) 1109–1112.
67. H.H. Joachin, S. Amiruddin, B. Li, T.D. Kaun, K. Amine, J. Prakash, *ECS Trans.*, 11 (2008) 13–18.